Electronic phase diagram of half-doped perovskite manganites on the plane of quenched disorder versus one-electron bandwidth

Y. Tomioka, T. Ito, and A. Sawa

Electronics and Photonics Research Institute, National Institute for Advanced Industrial Science and Technology (AIST),
1-1-1 Higashi, Tsukuba 305–8565, Japan

For half-doped manganese oxides that have a perovskite structure, $RE_{1-x}AE_x\mathrm{MnO_3}$ ($x = 0.5$) (RE and AE are rare-earth and alkaline-earth elements, respectively), the phase competition (stability) between the antiferromagnetic charge- or orbital-ordered insulator (CO/OO AFI), ferromagnetic metal (FM), layered (A-type) antiferromagnetic phase [AF(A)], and spin-glass-like insulator (SGI), have been studied using single crystals prepared by the floating zone method. The CO/OO AFI, FM, AF(A), and SGI are displayed on the plane of the disorder (the variance of the RE and AE cations) versus the effective one-electron bandwidth (the averaged ionic radius of the RE and AE). In the plane of the disorder versus the effective one-electron bandwidth, similar to the phase diagram of $RE_{1-x}AE_x\mathrm{MnO_3}$ ($x = 0.45$), the CO/OO AFI, FM, and SGI dominate at the lower-left, right, and upper regions, respectively. However, the CO/OO AFI for $x = 0.5$ is more stable than that for $x = 0.45$, and it expands to the plane points that correspond to the $RE_{0.5}\mathrm{Sr}_{0.5}\mathrm{MnO_3}$ ($RE = $ Nd and Sm) specimens as the hole concentration is commensurate with the ordering of $\mathrm{Mn^{3+}}/\mathrm{Mn^{4+}}$ with a ratio of 1/1. The y-dependent electronic phases for $RE_{0.5}(\mathrm{Sr}_{1-y}\mathrm{Ba}_y)_{0.5}\mathrm{MnO_3}$ ($0 \leqslant y \leqslant 0.5$) ($RE = $ Sm, $\mathrm{Nd}_{0.5}\mathrm{Sm}_{0.5}$, Nd, and Pr) show that the AF(A) intervenes between the CO/OO AFI and FM. Besides the region around $(\mathrm{La}_{1-y}\mathrm{Pr}_y)_{0.5}\mathrm{Sr}_{0.5}\mathrm{MnO_3}$ ($0 \leqslant y \leqslant 1$) that has a smaller disorder, the AF(A) also exists at the regions around $RE_{0.5}(\mathrm{Sr}_{1-y}\mathrm{Ba}_y)_{0.5}\mathrm{MnO_3}$ ($0 < y < 0.3$) ($RE = $ Sm and $\mathrm{Nd}_{0.5}\mathrm{Sm}_{0.5}$) that have a relatively larger disorder. This indicates that the AF(A) is rather robust against the increased disorder, even though an ordering of the $(x^2 - y^2)$ orbital occurs. This study has comprehensively investigated the effects of the disorder on the AF(A) as well as on the competition between the CO/OO AFI, FM, and AF(A) that is unique to $x = 0.5$. The comparison of phase diagrams between $x = 0.45$ and 0.5 brings further insights into the understanding of the rich electronic phases of manganites.

I. INTRODUCTION

Over the past decade, hole-doped manganese oxides that have a perovskite structure $RE_{1-x}AE_x\mathrm{MnO_3}$ (where RE and AE are rare-earth and alkaline earth elements, respectively) have been extensively studied owing to their promising magnetic and electronic properties including colossal magnetoresistance (CMR) [1,2]. The presence of the metallic ferromagnetism owing to double exchange (DE) interaction [3–7], as well as the antiferromagnetic insulating state that has a charge or orbital correlation are of fundamental importance for the properties of the materials. The critical temperature of the DE ferromagnetism depends on the effective one-electron bandwidth of the e_g band (W), or the transfer interactions of the e_g state carriers between neighboring Mn sites. In $RE_{1-x}AE_x\mathrm{MnO_3}$, the W depends on the crystal lattice distortion of the perovskite structure [8], or the tilting angle of the $\mathrm{MnO_6}$ octahedra, which can be controlled by the averaged ionic radius r_A of RE^{3+} and AE^{2+}, expressed as $r_A = (1 - x)r_{\mathrm{RE3+}} + x\, r_{\mathrm{AE2+}}$, where $r_{\mathrm{RE3+}}$ and $r_{\mathrm{AE2+}}$ are the ionic radii of the RE^{3+} and AE^{2+} cations. A decrease of the r_A leads to an increase of the lattice distortion, which consequently yields a narrow W. It has been shown that in the distorted manganites that have a narrow W (e.g., $\mathrm{Pr}_{1-x}\mathrm{Ca}_x\mathrm{MnO_3}$), instead of the ferromagnetic metal (FM) due to the DE, an insulator that has a real space ordering of $\mathrm{Mn^{3+}}/\mathrm{Mn^{4+}}$ with a ratio of 1/1 accompanied with an ordering of the e_g orbital

[charge-, or orbital-ordered insulator (CO/OOI)] appears for $0.3 \leqslant x < 0.75$ [9–12].

For the half-doped manganites, or when $x \geqslant 0.5$, besides the above phases of CO/OOI and FM, a layered (A-type [13]) antiferromagnetic phase [AF(A)] becomes energetically favorable as well, as indicated both experimentally as well as theoretically. [14–19] In $\mathrm{Pr}_{0.5}\mathrm{Ca}_x\mathrm{Sr}_{0.5-x}\mathrm{MnO_3}$ [16] and $\mathrm{La}_{0.5}\mathrm{Ca}_{0.5-x}\mathrm{Sr}_x\mathrm{MnO_3}$ [17–19], the low-temperature phase changes from the CO/OOI with the antiferromagnetic CE-type structure [13] (CO/OO AFI) for the Ca-rich compounds to the AF(A) for the Sr-rich ones. For $x = 0.5$, there is a competition between the CO/OO AFI, FM, and AF(A). The situation is simpler when $x = 0.45$, where there is a competition only between the CO/OO AFI and FM [20].

Besides the effective one-electron bandwidth, the quenched disorder upon the substitution of RE^{3+} with AE^{2+} is also a key factor that modifies the electronic phases of manganites. This can lead to a reduction of the Curie temperature [21,22], an appearance of a spin-glass-like insulator (SGI) [23], and a suppression of the first-order nature of the transition [24,25]. The quenched disorder is evaluated by the variance σ^2 of the ionic radii of the RE^{3+} and AE^{2+} cations, defined as $\sigma^2 = \Sigma(x_i r_i^2 - r_A^2)$, where x_i and r_i are the fractional occupancies and the ionic radii of the RE^{3+} and AE^{2+}, respectively. In relation to the above effects that arise due to the disorder, a resultant electronic phase separation has been studied and related to the origin of CMR [25–28]. The comparison of phase

diagrams between $RE_{0.5}Ba_{0.5}MnO_3$ [29] and REBaMn$_2$O$_6$ [30] has further indicated that the CO/OO AFI is more strongly suppressed by the disorder compared to the FM [31]. The effect of the disorder on the CO/OO AFI and FM, competing with each other, has been extensively investigated.

As indicated in the temperature versus the hole concentration ($T - x$) phase diagrams of $RE_{1-x}Sr_xMnO_3$ ($RE =$ Nd [32], Sm [12,33], and Eu [34]), the AF(A) becomes dominant for $x \geqslant 0.5$. The critical temperature for the AF(A) depends on the r_A, or the W, similarly to that of the FM. However, within the ferromagnetic plane of the AF(A), an ordering of the ($x^2 - y^2$) orbital occurs [14]. The effects of the disorder on the AF(A) as well as on the phase competition between the CO/OOI, FM, and AF(A) that is unique to the case when $x = 0.5$ have not been sufficiently investigated. An investigation of the electronic phases for $x = 0.5$ as functions of the quenched disorder and the effective one-electron bandwidth is desirable to comprehensively understand what is described above. Especially, an effect of the disorder on the AF(A) that is a two-dimensional ferromagnet accompanied with the ($x^2 - y^2$) orbital ordering is considered to be of interest.

In this study, we investigate the phase competition (stability) between the CO/OO AFI, FM, and AF(A) for various $RE_{1-x}AE_xMnO_3$ ($x = 0.5$) single crystals prepared using the floating zone method. After the description of the experimental procedures in Sec. II, in Sec. III A, we show the phase diagram of $RE_{1-x}AE_xMnO_3$ ($x = 0.5$) on the plane of the σ^2 versus the r_A. In the phase diagram, one can see that the AF(A) appears between the area of the CO/OO AFI and that of the FM. In Secs. III B and III C, we show the experimental data used to construct the phase diagram. In Sec. III B, the y-dependent electronic phases of $RE_{0.5}(Ca_{1-y}Sr_y)_{0.5}MnO_3$ ($0 \leqslant y \leqslant 1$) with $RE =$ Gd, Sm, and Nd, are discussed. In the phase diagram on the plane of the σ^2 versus the r_A, these specimens are located at the lower-left ($r_A < 1.35$ Å and $\sigma^2 < 0.012$ Å^2) regions where the CO/OO AFI dominates. In Sec. III C, the electronic phases of $RE_{0.5}(Sr_{1-y}Ba_y)_{0.5}MnO_3$ ($0 \leqslant y \leqslant 0.5$) with $RE =$ Sm, Nd$_{0.5}$Sm$_{0.5}$, Nd, and Pr, are discussed. In the phase diagram, these specimens are located at the right-hand regions where the AF(A) appears. The summary is given in Sec. IV.

II. EXPERIMENTAL METHODS

Single crystals of the half-doped manganites, except for $RE_{0.5}AE_{0.5}MnO_3$ ($RE =$ Y and La, $AE =$ Ca and Sr) and the series of La$_{0.5}$(Ca$_{1-y}$Sr$_y$)$_{0.5}$MnO$_3$ ($0 \leqslant y \leqslant 1$), were prepared using the floating zone method. The crystal growth methods are reported in Refs. [35,36]. The magnetization up to a value of 7 T was measured using a superconducting quantum interference device (SQUID) magnetometer [Magnetic Property Measurement System (MPMS), Quantum Design Inc.]. Once the crystal was cooled down to the lowest temperature in zero field, the magnetic field was settled, and the zero-field-cooled (ZFC) magnetization was measured with the increase of the temperature. The field-cooled (FC) magnetization was subsequently measured by decreasing the temperature in the presence of the same magnetic field. The magnetic field was applied along an arbitrary direction with respect to the crystallographic axes. Resistivity as well as the ac susceptibility were measured in

a cryostat [Physical Property Measurement System (PPMS), Quantum Design Inc.]. The transport current was injected in an arbitrary direction with respect to the crystallographic axes. The ac susceptibility was measured by changing the frequency from 500 Hz to 10 kHz. The excitation field (H_{ac}) was 10 Oe.

III. RESULTS AND DISCUSSION

A. Phase diagram plotted on the plane of the quenched disorder versus the one-electron bandwidth

Figure 1 shows the transition temperatures T_{CO}, T_C, $T_N(A)$, and T_G that correspond to the CO/OO AFI, FM, AF(A), and SGI, respectively, for various $RE_{1-x}AE_xMnO_3$ ($x = 0.5$) specimens, as well as the obtained electronic phase diagram on the plane of the quenched disorder (σ^2) versus the one-electron bandwidth (r_A). The temperatures T_{CO}, T_C, and $T_N(A)$ were determined using the corresponding anomalies in the temperature profiles of the resistivity at which $|d\ln(\rho)/d(1/T)|$ (ρ is the resistivity) has the maximum value. The values shown in Fig. 1 are averaged between the cooling and heating runs. The T_G was determined using the local maximum of the temperature profiles of the ac susceptibility measured at 500 Hz, or using the cusp structure of the ZFC magnetization at 100 Oe. Note that in the figure, the transition temperatures for $RE_{0.5}AE_{0.5}MnO_3$ ($RE =$ Y and La, $AE =$ Ca and Sr) [37–40], La$_{0.5}$Ca$_{0.5-x}$Sr$_x$MnO$_3$ ($x = 0.2$, 0.3, and 0.4) [17–19], Pr$_{0.5}$(Ca$_{1-y}$Sr$_y$)$_{0.5}$MnO$_3$ [35], and (Nd$_{1-y}$Sm$_y$)$_{0.5}$Sr$_{0.5}$MnO$_3$ ($y = 0$, 0.25, 0.5, and 0.75) [41,42] are taken from the corresponding cited literature. In Fig. 1, similar to the phase diagram of $RE_{1-x}AE_xMnO_3$ ($x = 0.45$) [20], the CO/OO AFI, FM, and SGI phases dominate at the lower-left ($r_A < 1.35$ Å and $\sigma^2 < 0.012$ Å^2), right, and upper regions, respectively. However, the area of the CO/OO AFI for $x = 0.5$ is more extended than that for $x = 0.45$, and reaches the points that present the specimens of $RE_{0.5}Sr_{0.5}MnO_3$ ($RE =$ Sm and Nd). The CO/OO AFI for $x = 0.5$ is more stable than that for $x = 0.45$, as the hole concentration is commensurate with the ordering of Mn^{3+}/Mn^{4+} with a ratio of 1/1. In addition, Fig. 1 shows that the AF(A) intervenes between the CO/OO AFI and FM. Besides the region around (La$_{1-y}$Pr$_y$)$_{0.5}$Sr$_{0.5}$MnO$_3$ ($0 \leqslant y \leqslant 1$) that has a smaller amount of disorder, one can see that the AF(A) also exists in the regions around Sm$_{0.5}$(Sr$_{1-y}$Ba$_y$)$_{0.5}$MnO$_3$ ($0 < y < 0.2$) and (Nd$_{0.5}$Sm$_{0.5}$)$_{0.5}$(Sr$_{1-y}$Ba$_y$)$_{0.5}$MnO$_3$ ($0.1 \leqslant y \leqslant 0.2$) that have a relatively larger amount of disorder.

B. Charge or orbital ordering of $RE_{0.5}(Ca_{1-y}Sr_y)_{0.5}MnO_3$ ($RE =$ Gd, Sm, and Nd)

Figure 2 shows the temperature profiles of the resistivity (a)–(c) and phase diagrams (d)–(f) for $RE_{0.5}(Ca_{1-y}Sr_y)_{0.5}MnO_3$ ($0 \leqslant y \leqslant 1$) with $RE =$ Gd [(a) and (d)], Sm [(b) and (e)], and Nd [(c) and (f)]. In Figs. 2(a)–2(c), the resistivities for $y = 0$ show anomalies around $\sim$290 (for $RE =$ Gd), $\sim$280 (for $RE =$ Sm), and $\sim$240 K (for $RE =$ Nd), respectively, in both heating and cooling runs, which indicates the transition to the CO/OOI. In Fig. 2(a) ($RE =$ Gd), the anomalies, i.e., the T_{CO}, shift to lower temperatures with the increase of y, as shown in the resistivity curve for $y = 0.1$ and 0.2. However, when
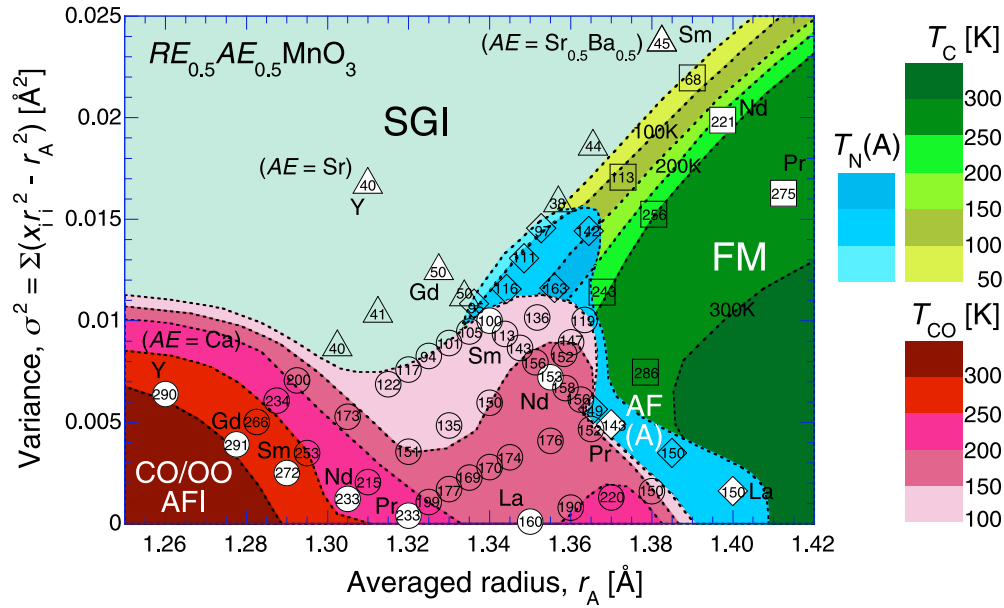
FIG. 1. The transition temperatures T_{CO} (circles), T_C (squares), $T_N(A)$ (diamonds), and T_G (triangles) that correspond to the charge- or orbital-ordered insulator (CO/OOI), the ferromagnetic metal (FM), the A-type antiferromagnetic phase [AF(A)], and the spin-glass-like insulator (SGI), respectively, for various $RE_{1-x}AE_xMnO_3$ ($x = 0.5$) specimens, as well as the obtained electronic phase diagram on the plane of the quenched disorder (σ^2) vs the one-electron bandwidth (r_A). The temperatures T_{CO}, T_C, and $T_N(A)$ were determined using the corresponding anomalies in the temperature profiles of the resistivity at which $|d\ln(\rho)/d(1/T)|$ (ρ is the resistivity) has the maximum value. The values are averaged between the cooling and heating runs. The T_G was determined using the local maximum of the temperature profiles of the ac susceptibility measured at 500 Hz, or using the cusp structure of the ZFC magnetization at 100 Oe. The points that correspond to the specimens, the RE^{3+} of which is not alloyed (e.g., La$_{0.5}$Sr$_{0.5}$MnO$_3$), are painted white. The contours of the transition temperatures for the CO/OO AFI, FM, and AF(A) are drawn based on the values written in this figure. Note that the transition temperatures for $RE_{0.5}AE_{0.5}MnO_3$ (RE = Y and La, AE = Ca and Sr) [37–40], La$_{0.5}$Ca$_{0.5-x}$Sr$_x$MnO$_3$ ($x = 0.2, 0.3$, and 0.4) [17–19], Pr$_{0.5}$(Ca$_{1-y}$Sr$_y$)$_{0.5}$MnO$_3$ [35], and (Nd$_{1-y}$Sm$_y$)$_{0.5}$Sr$_{0.5}$MnO$_3$ ($y = 0, 0.25, 0.5$, and 0.75) [41] are taken from the corresponding cited literature.

$y = 0.7$ or 1, such anomalies are not discerned. In the inset of Fig. 2(d), we show the ac susceptibility for a $y = 0.5$ crystal. In the inset, the ac susceptibility at 500 Hz shows a local maximum at ~40 K that shifts to higher temperatures as the frequency increases. Such frequency-dependent behavior of the ac susceptibility indicates that the $y = 0.5$ crystal undergoes a transition to the spin-glass-like state at ~40 K. Using the results shown in Fig. 2(a) as well as the inset of Fig. 2(d), the y-dependent phase diagram for RE = Gd is deduced, as shown in Fig. 2(d). The increase in y for the $RE_{0.5}$(Ca$_{1-y}$Sr$_y$)$_{0.5}$MnO$_3$ specimens represents a diagonal shift in the diagram in Fig. 1. When RE = Gd, the CO/OO AFI remains for $0 \leqslant y \leqslant 0.3$, however, it changes to SGI for $0.5 \leqslant y \leqslant 1$, as shown in Fig. 2(d).

In Fig. 2(b), for RE = Sm, similar to Fig. 2(a), the anomalies in the resistivity shift to lower temperatures with the increase of y. For $y = 0.3$, the T_{CO} is lowered to ~200 K, and the transition becomes broadened. For $y = 0.6$ and 0.9, the T_{CO} is lowered further to values of ~120 and ~100 K, respectively. Based on these results shown in Fig. 2(b), in Fig. 2(e) we show the phase diagram for RE = Sm. Note that when RE = Sm, although the T_{CO} is lowered with the increase in y, the CO/OO AFI remains the low-temperature phase for $0 \leqslant y \leqslant 1$, as shown in Fig. 2(e).

In Fig. 2(c) for RE = Nd, T_{CO} is lowered to approximately 215 K, as shown in the resistivity curve for $y = 0.1$. For $y = 0.3$, the resistivity shows a decreasing at ~180 K, however, it

shows an intense increase at 120 K on cooling, i.e., the FM that has a $T_C \sim 180$ K undergoes a transition to CO/OO AFI at 120 K. In the heating run, the resistivity shows a decrease only at ~190 K, which indicates that the CO/OO AFI changes to a paramagnetic insulating state at 180 K without changing to FM. For $y = 0.5$ and 0.7, the FM appears at ~200 and ~220 K, respectively. However, it is replaced with CO/OO AFI at lower temperatures [41]. These features [Fig. 2(c)] are summarized in the phase diagram for RE = Nd [Fig. 2(f)]. As shown in Fig. 2(f), although the FM starts to emerge for $y \geqslant 0.3$ at a higher temperature, and the T_C increases with y, the CO/OO AFI dominates the low-temperature phase for $0 \leqslant y \leqslant 1$.

For $RE_{0.5}$(Ca$_{1-y}$Sr$_y$)$_{0.5}$MnO$_3$ $(0 \leqslant y \leqslant 1)$ $(RE =$ Gd, Sm, and Nd), even though the SGI emerges at $0.5 \leqslant y \leqslant 1$ for RE = Gd, the CO/OO AFI dominates the low-temperature phase, as shown in Figs. 2(d)–2(f).

C. A-type antiferromagnetic phase of $RE_{0.5}$(Sr$_{1-y}$Ba$_y$)$_{0.5}$MnO$_3$ $(0 \leqslant y \leqslant 0.5)$ $(RE =$ Sm, Nd$_{0.5}$Sm$_{0.5}$, Nd, and Pr)

Figure 3 shows the temperature profiles of resistivity (a)–(d) as well as the phase diagrams (e)–(h) for $RE_{0.5}$(Sr$_{1-y}$Ba$_y$)$_{0.5}$MnO$_3$ $(0 \leqslant y \leqslant 0.5)$ with RE = Sm [(a) and (e)], Nd$_{0.5}$Sm$_{0.5}$ [(b) and (f)], Nd [(c) and (g)], and Pr [(d) and (h)]. In Fig. 3(a) for RE = Sm, the resistivity for $y = 0$ exhibits a transition to AF(A) at ~130 K, and to CO/OO AFI at ~100 K [36]. For $y = 0.05$, the resistivity shows a decrease
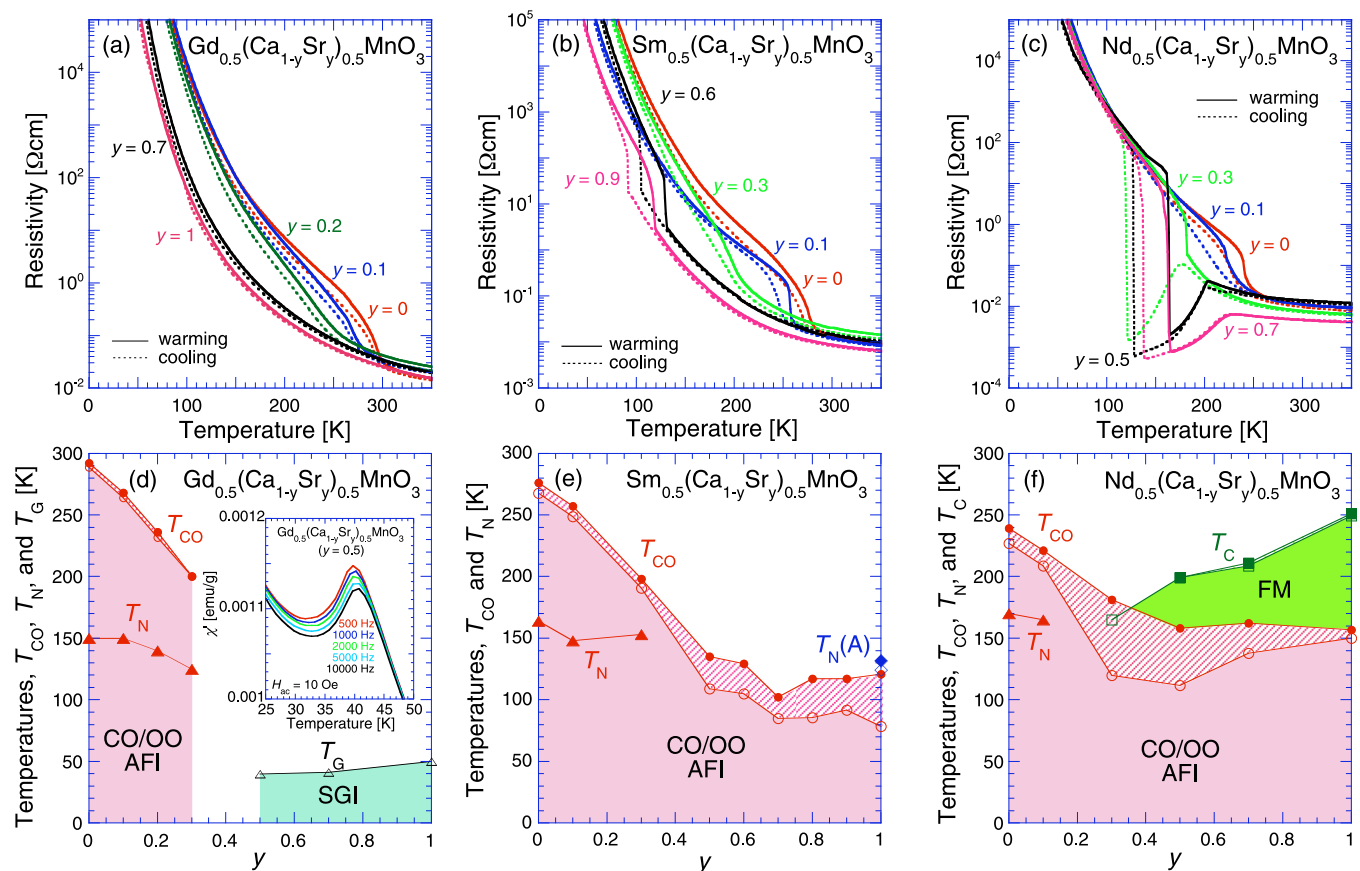
FIG. 2. The temperature profiles of the resistivity (a)–(c) and the phase diagrams (d)–(f) for $RE_{0.5}(Ca_{1-y}Sr_y)_{0.5}MnO_3$ ($0 \leqslant y \leqslant 1$) with RE = Gd [(a) and (d)], Sm [(b) and (e)], and Nd [(c) and (f)]. The temperatures T_{CO} (circles), T_C (squares), $T_N(A)$ (diamonds), and T_G (triangles) for the CO/OO AFI, FM, AF(A), and SGI, respectively, were determined in the same manner that is described in the captions of Fig. 1. Open and closed symbols are the temperatures determined from the temperature profiles of the resistivity in the cooling and heating runs, respectively. The hysteresis regions are hatched. The Neel temperatures for the *CE*-type antiferromagnetic state are denoted as closed triangles. The inset of (d) indicates the temperature profiles of ac susceptibility for a $Gd_{0.5}(Ca_{1-y}Sr_y)_{0.5}MnO_3$ ($y = 0.5$) crystal.

around 120 K on cooling, which indicates the transition to AF(A). A similar resistive behavior is observed for the $y = 0.1$ crystal. The CO/OO AFI at $y = 0$ is removed for $y \geqslant 0.05$. For $y = 0.2$, a subtle anomaly can be observed around 120 K, which is likely due to the transition to an AF(A). However, in the analysis of the temperature profiles of the resistivity, $|d\ln(\rho)/d(1/T)|$ has not shown a local maximum around 120 K. For $y = 0.3$, the resistivity has no anomalies, hence keeping the insulating behavior down to 50 K. In the inset of Fig. 3(a), we show the temperature profiles of magnetization for the crystals with $y = 0.1$, 0.2, and 0.3. In the inset, the magnetization for $y = 0.1$ shows a distinct decrease at $\sim$120 K [$T_N(A)$] in the data collected on cooling, which is consistent with the resistivity for $y = 0.1$ shown in Fig. 3(a). For $y = 0.2$, although a relatively gradual decrease in magnetization is observed around 100 K in the cooling run, a discrepancy between ZFC and FC magnetization can be noticed below $\sim$30 K. In addition, the ZFC magnetization shows a cusp structure around 20 K, which indicates the transition to a spin-glass-like state. For $y = 0.3$, shown in the inset, the decrease in magnetization is not observed. In addition, the discrepancy between the ZFC and FC magnetization becomes pronounced below $\sim$50 K. These results shown in Fig. 3(a) and its inset

are summarized in Fig. 3(e) that shows the electronic phases as a function of y for $Sm_{0.5}(Sr_{1-y}Ba_y)_{0.5}MnO_3$ ($0 \leqslant y \leqslant 0.5$). As shown in Fig. 3(e), the CO/OO AFI at $y = 0$ changes to AF(A) for $0 < y < 0.2$. For $0.2 \leqslant y \leqslant 0.5$, the SGI dominates in the low-temperature phase, most likely due to the increased disorder.

In Fig. 3(b), for $RE = Nd_{0.5}Sm_{0.5}$, the resistivity for $y = 0.05$ reflects the transition to CO/OO AFI around 135 K, followed by a transition to FM at $\sim$185 K, similar to the case when $y = 0$ [41]. However, for $y = 0.1$ and 0.2, the resistivity shows a decrease at $\sim$165 and $\sim$145 K in the cooling run, respectively, which indicates the transition to an AF(A). For these crystals, neither CO/OO AFI nor FM are manifested for the whole temperature region. The CO/OO AFI is removed for $y > 0.05$, and it is replaced with AF(A), similar to the case for $RE = $ Sm [Fig. 3(a)]. On the other hand, for $y = 0.3$ and 0.5, the FMs with $T_C \sim 115$ and $\sim$70 K, respectively, are recovered. In this figure, the value of the resistivity at low temperatures for $y = 0.5$ is not sufficiently low as that for a FM, which indicates that both FM and SGI coexist for $y = 0.5$. However, for $y = 0.5$, taking into account that the estimate for the saturation magnetization at 5 K is $\sim$3.0 [μ_B/Mn site], a larger part of the specimen is considered as
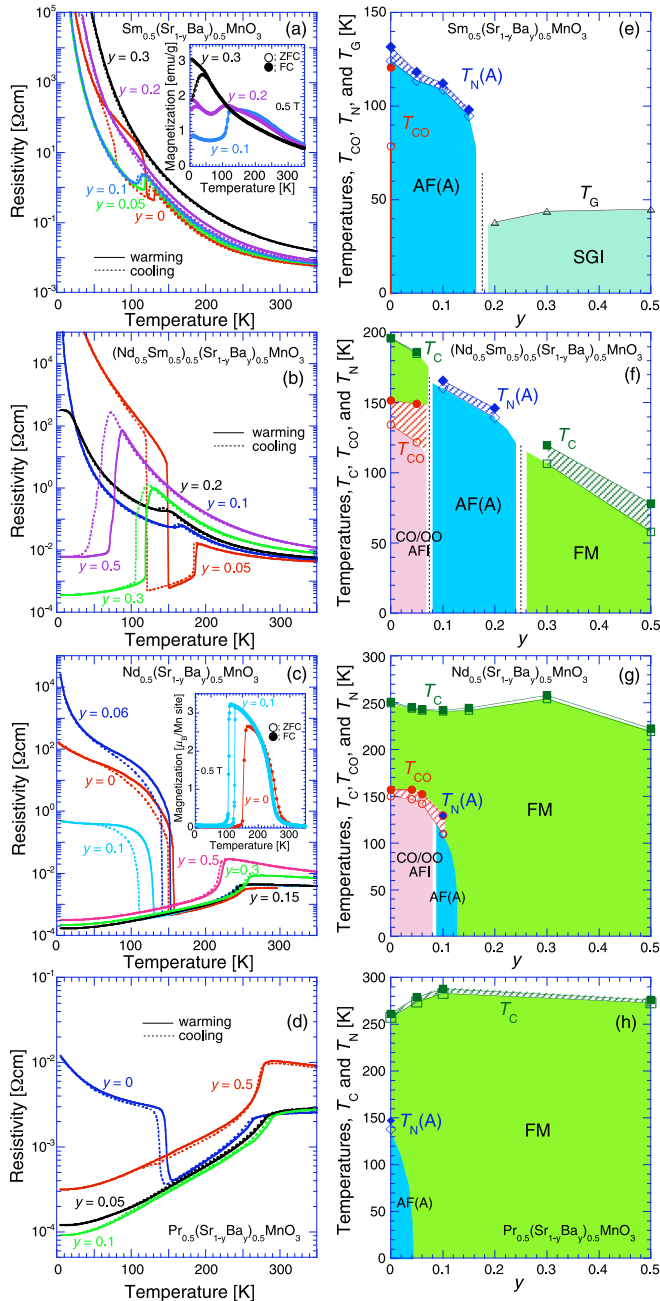
FIG. 3. The temperature profiles of the resistivity (a)–(d) and the phase diagrams (e)–(h) for $RE_{0.5}(Sr_{1-y}Ba_y)_{0.5}MnO_3$ ($0 \leqslant y \leqslant 0.5$) with RE = Sm [(a) and (e)], $Nd_{0.5}Sm_{0.5}$ [(b) and (f)], Nd [(c) and (g)], and Pr [(d) and (h)]. The temperatures T_{CO}, T_C, $T_N(A)$, and T_G for the CO/OO AFI, FM, AF(A), and SGI, respectively, were determined in the same manner that is described in the captions of Fig. 1. Open and closed symbols are the temperatures determined from the temperature profiles of the resistivity in the cooling and heating runs, respectively. The hysteresis regions are hatched. The insets of (a) and (c) are the temperature profiles of magnetization at 0.5 T for the crystals of $Sm_{0.5}(Sr_{1-y}Ba_y)_{0.5}MnO_3$ ($y = 0.1$, 0.2, and 0.3) (a) and $Nd_{0.5}(Sr_{1-y}Ba_y)_{0.5}MnO_3$ ($y = 0$ and 0.1) (c), respectively.

FM. Figure 3(f) shows the electronic phases as a function of y for $(Nd_{0.5}Sm_{0.5})_{0.5}(Sr_{1-y}Ba_y)_{0.5}MnO_3$ ($0 \leqslant y \leqslant 0.5$), obtained using the results in Fig. 3(b). As shown in Fig. 3(f),

although the CO/OO AFI remains for $0 \leqslant y \leqslant 0.05$, AF(A) is the low-temperature phase for $0.1 \leqslant y \leqslant 0.2$, while FM is for $0.3 \leqslant y \leqslant 0.5$.

In Fig. 3(c) for RE = Nd, the resistivity for $y = 0.06$ reflects the transition to an insulating state around 145 K, followed by a transition to FM at $\sim$250 K, similar to the resistive behavior when $y = 0$ [42]. Taking into account that the resistivity value at the insulating state for $y = 0.06$ is comparable with, or higher than that for $y = 0$, the low-temperature phase for $y = 0.06$ is considered to be the CO/OO AFI. Similar to the cases when $y = 0$ and 0.06, the resistivity for $y = 0.1$ also reflects the transition from FM to a high-resistive state around 120 K. However, the resistivity value at the high-resistive state for $y = 0.1$ is considerably lower than that for $y = 0$. In the inset of Fig. 3(c), we show the temperature profiles of magnetization for the crystals with $y = 0$ and 0.1. The inset shows that the magnetization value at low temperatures for $y = 0.1$ is comparable with that for $y = 0$, which indicates that no residual FM remains at low temperatures. In an AF(A), a ferromagnetic plane is antiferromagnetically coupled with the neighboring plane [14,43], and the resistivity of the AF(A) is lower than that of the CO/OO AFI that has the antiferromagnetic CE-type spin-ordering. Therefore the lower value of the resistivity for $y = 0.1$ in Fig. 3(c) implies that the AF(A) is included in the low-temperature phase for $y = 0.1$. With a further increase of y [Fig. 3(c)], for $y = 0.15$, 0.3, and 0.5, the FMs with $T_C \sim$ 250, $\sim$260, and $\sim$220 K, respectively, are present down to the lowest temperature without appearances of a CO/OO AFI or an AF(A). Using these results in Fig. 3(c) and its inset, the y-dependent electronic phase for $Nd_{0.5}(Sr_{1-y}Ba_y)_{0.5}MnO_3$ ($0 \leqslant y \leqslant 0.5$) is deduced, as shown in Fig. 3(g), where the CO/OO AFI remains at $0 \leqslant y < 0.1$, while FM becomes dominant for $0.1 < y \leqslant 0.5$. Both CO/OO AFI and AF(A) are considered to coexist around $y = 0.1$.

In Fig. 3(d) for RE = Pr, the resistivity for $y = 0$ reflects the transition from FM to AF(A) around 140 K, followed by a transition to FM at $\sim$260 K [44]. For $y = 0.05$, the resistivity reflects the transition to FM, which is manifested by the anomaly at $\sim$280 K. However, it does not show a transition to an AF(A), hence the FM remains down to the lowest temperature. With a further increase in y, for $y = 0.1$ and 0.5, the FMs with $T_C \sim$ 290 and $\sim$270 K, respectively, remain down to the lowest temperature. Based on the results in Fig. 3(d), the electronic phases as a function of y for $Pr_{0.5}(Sr_{1-y}Ba_y)_{0.5}MnO_3$ ($0 \leqslant y \leqslant 0.5$) are shown in Fig. 3(h). Even though the AF(A) exists at $y = 0$ as the low temperature phase, the FM dominates for $0.05 \leqslant y \leqslant 0.5$.

Next, we discuss the phase change from AF(A) to SGI for $(Sm_{1-y}Gd_y)_{0.5}Sr_{0.5}MnO_3$ ($y = 0.3$ and 0.5) and that from AF(A) to CO/OO AFI for $(Pr_{1-y}Nd_y)_{0.5}Sr_{0.5}MnO_3$ ($y = 0.4$ and 0.45). In Fig. 4, we show the temperature profiles of the resistivity for the crystals of $(Sm_{1-y}Gd_y)_{0.5}Sr_{0.5}MnO_3$ ($y = 0.3$ and 0.5) (a) and $(Pr_{1-y}Nd_y)_{0.5}Sr_{0.5}MnO_3$ ($y = 0.4$ and 0.45) (b). In addition, in Fig. 4(b), the resistivity of the $(La_{0.5}Pr_{0.5})_{0.5}Sr_{0.5}MnO_3$ crystal is shown.

In Fig. 4(a), for $y = 0.3$, the resistivity shows a decrease at 100 K in the cooling run, and concomitantly, the magnetization shows a steep decrease at the same temperature, as shown in
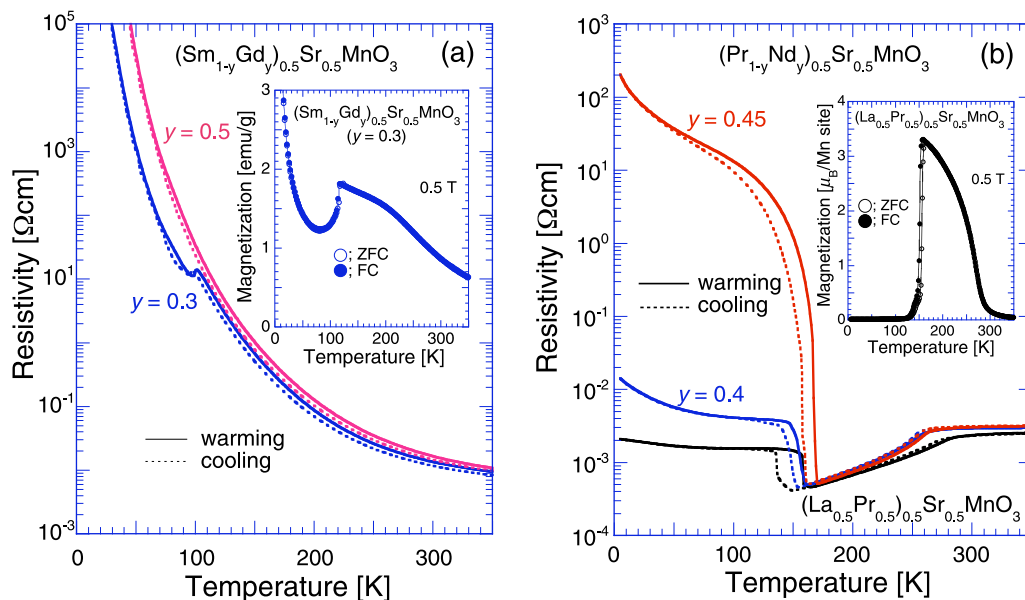
FIG. 4. The temperature profiles of the resistivity for the crystals of $(Sm_{1-y}Gd_y)_{0.5}Sr_{0.5}MnO_3$ ($y = 0.3$ and 0.5) (a) and $(Pr_{1-y}Nd_y)_{0.5}Sr_{0.5}MnO_3$ ($y = 0.4$ and 0.45) (b). In (b), the temperature profiles of the resistivity for a $(La_{0.5}Pr_{0.5})_{0.5}Sr_{0.5}MnO_3$ crystal are also shown. The insets of (a) and (b) indicate the temperature profiles of magnetization at 0.5 T for the crystals of $(Sm_{1-y}Gd_y)_{0.5}Sr_{0.5}MnO_3$ ($y = 0.3$) (a) and $(La_{0.5}Pr_{0.5})_{0.5}Sr_{0.5}MnO_3$ (b), respectively.

the inset, which indicates that the $y = 0.3$ crystal undergoes a transition to an AF(A). On the other hand, the resistivity of the $y = 0.5$ crystal does not show anomalies, hence the insulating behavior remains down to 50 K. This indicates that the low-temperature phase for $y = 0.5$ is a SGI. Figures 4(a) and 3(a) indicate that for $(Sm_{1-y}Gd_y)_{0.5}Sr_{0.5}MnO_3$ ($0 \leqslant y \leqslant 1$), the CO/OO AFI changes to AF(A) at $0 < y < 0.3$, and the AF(A) changes to SGI at $0.3 < y < 0.5$.

In Fig. 4(b), the resistivity for a $(La_{0.5}Pr_{0.5})_{0.5}Sr_{0.5}MnO_3$ crystal shows an anomaly around $\sim$280 K, which indicates the transition to FM. It further shows a steep increase (decrease) around 135 K (160 K) on cooling (heating). The resistivity value at low temperatures is in the order of mΩcm, comparable with that of $Pr_{0.5}(Sr_{1-y}Ba_y)_{0.5}MnO_3$ ($y = 0$) shown in Fig. 3(d). The temperature profile of the magnetization for a $(La_{0.5}Pr_{0.5})_{0.5}Sr_{0.5}MnO_3$ crystal is shown in the inset of Fig. 4(b). In relation to the resistive transition, the magnetization starts to decrease around 150 K in the cooling run, as shown in the inset. These features of the resistivity and magnetization suggest that the $(La_{0.5}Pr_{0.5})_{0.5}Sr_{0.5}MnO_3$ crystal undergoes a transition from a FM to an AF(A) around 150 K.

In Fig. 4(b), for $(Pr_{1-y}Nd_y)_{0.5}Sr_{0.5}MnO_3$, similar to the case of $(La_{0.5}Pr_{0.5})_{0.5}Sr_{0.5}MnO_3$, the resistivities for $y = 0.4$ and 0.45 reflect the transitions to an insulating state around 155 and 165 K, respectively, followed by a transition to FM at $\sim$260 K. The resistivity value of the insulating state for $y = 0.4$ is comparable with those of $(La_{0.5}Pr_{0.5})_{0.5}Sr_{0.5}MnO_3$ and $Pr_{0.5}(Sr_{1-y}Ba_y)_{0.5}MnO_3$ ($y = 0$) [Fig. 3(d)], however, it is much lower than those of $y = 0.45$ and $Nd_{0.5}(Sr_{1-y}Ba_y)_{0.5}MnO_3$ ($y = 0$) [Fig. 3(c)]. This large difference in resistivity at the insulating state between $y = 0.4$ and 0.45 implies that the low-temperature phase is an AF(A) for $y = 0.4$, while it is the CO/OO AFI for $y = 0.45$. Figures 4(b), 3(d), and 3(c) indicate that for $(Pr_{1-y}Nd_y)_{0.5}Sr_{0.5}MnO_3$ ($0 \leqslant y \leqslant 1$), the low-temperature phase is an AF(A) for $0 \leqslant y \leqslant 0.4$, while it is the CO/OO AFI for $0.45 \leqslant y \leqslant 1$.

IV. SUMMARY

The phase competition (stability) between the antiferromagnetic charge- or orbital-ordered insulator (CO/OO AFI), the ferromagnetic metal (FM), the A-type antiferromagneic state [AF(A)], and a spin-glass-like insulator (SGI) has been studied for the half-doped manganites, $RE_{1-x}AE_xMnO_3$ ($x = 0.5$). The quenched disorder and the effective one-electron bandwidth are experimentally evaluated by the variance σ^2 and the averaged ionic radius r_A of the RE^{3+} and AE^{2+} cations, respectively. The CO/OO AFI, FM, AF(A), and SGI have been displayed on the plane of the quenched disorder (σ^2) versus the effective one-electron bandwidth (r_A).

In the plane of the σ^2 versus the r_A, similar to the electronic phase diagram of $RE_{1-x}AE_xMnO_3$ ($x = 0.45$), the CO/OO AFI, FM, and SGI dominate at the lower-left, right, and upper regions, respectively. However, the CO/OO AFI for $x = 0.5$ is more stable than that for $x = 0.45$, and the area of the CO/OO AFI for $x = 0.5$ expands to the plane points that correspond to the specimens of $RE_{0.5}Sr_{0.5}MnO_3$ ($RE =$ Sm and Nd) as the hole concentration is commensurate with the ordering of Mn^{3+}/Mn^{4+} with 1/1. The y-dependent electronic phases for $RE_{0.5}(Sr_{1-y}Ba_y)_{0.5}MnO_3$ ($0 \leqslant y \leqslant 0.5$) ($RE =$ Sm, $Nd_{0.5}Sm_{0.5}$, Nd, and Pr) have shown that the AF(A) intervenes between the CO/OO AFI and FM.

We have comprehensively investigated the effects of the disorder on the AF(A) as well as on the competition between the CO/OO AFI, FM, and AF(A) that is unique to $x = 0.5$. This study, together with the phase diagram of $x = 0.45$, brings further insights into the understanding of the rich electronic phases of manganites.

[1] E. Dagotto, T. Hotta, and A. Moreo, Phys. Rep. **344**, 1 (2001).

[2] Y. Tokura, Rep. Prog. Phys. **69**, 797 (2006).

[3] G. H. Jonker and J. H. van Santen, Physica **16**, 337 (1950).

[4] G. H. Jonker, Physica **22**, 707 (1956).

[5] C. Zener, Phys. Rev. **82**, 403 (1951).

[6] P. W. Anderson and H. Hasegawa, Phys. Rev. **100**, 675 (1955).

[7] P. -G. de Gennes, Phys. Rev. **118**, 141 (1960).

[8] J. B. Torrance, P. Lacorre, A. I. Nazzal, E. J. Ansaldo, and Ch. Niedermayer, Phys. Rev. B **45**, 8209 (1992).

[9] E. Pollert, S. Krupicka, and E. Kuzmicova, J. Phys. Chem. Solids **43**, 1137 (1982).

[10] Z. Jirak, S. Krupicka, V. Nekvasil, E. Pollert, G. Villeneuve, and F. Zounova, J. Magn. Magn. Mater. **15–18**, 519 (1980).

[11] Z. Jirak, S. Krupicka, Z. Simsa, M. Dlouha, and Z. Vratislav, J. Magn. Magn. Mater. **53**, 153 (1985).

[12] C. Martin, A. Maignan, M. Hervieu, and B. Raveau, Phys. Rev. B **60**, 12191 (1999).

[13] E. O. Wollan and W. C. Koehler, Phys. Rev. **100**, 545 (1955).

[14] A. Taraphder, J. Phys. Condens. Matter **19**, 125218 (2007), and references therein.

[15] S. Yunoki, T. Hotta, and E. Dagotto, Phys. Rev. Lett. **84**, 3714 (2000).

[16] F. Damay, Z. Jirak, M. Hervieu, C. Martin, A. Maignan, B. Raveau, G. Andre, and F. Bouree, J. Magn. Magn. Mater. **190**, 221 (1998); Z. Jirak, F. Damay, M. Hervieu, C. Martin, B. Raveau, G. Andre, and F. Bouree, Phys. Rev. B **61**, 1181 (2000).

[17] A. Sundaresan, P. L. Paulose, R. Mallik, and E. V. Sampathkumaran, Phys. Rev. B **57**, 2690 (1998).

[18] I. Dhiman, A. Das, P. K. Mishra, and L. Panicker, Phys. Rev. B **77**, 094440 (2008).

[19] I. Dhiman, A. Das, R. Mittal, Y. Su, A. Kumar, and A. Radulescu, Phys. Rev. B **81**, 104423 (2010).

[20] Y. Tomioka and Y. Tokura, Phys. Rev. B **70**, 014432 (2004).

[21] L. M. Rodriguez-Martinez and J. P. Attfield, Phys. Rev. B **54**, 15622(R) (1996).

[22] L. M. Rodriguez-Martinez and J. P. Attfield, Phys. Rev. B **63**, 024424 (2000).

[23] T. Terai, T. Sasaki, T. Kakeshita, T. Fukuda, T. Saburi, H. Kitagawa, K. Kindo, and M. Honda, Phys. Rev. B **61**, 3488 (2000).

[24] M. Otero-Leal, F. Rivadulla, and J. Rivas, Phys. Rev. B **76**, 174413 (2007).

[25] J. Burgy, M. Mayr, V. Martin-Mayor, A. Moreo, and E. Dagotto, Phys. Rev. Lett. **87**, 277202 (2001).

[26] M. Uehara, S. Mori, C. H. Chen, and S.-W. Cheong, Nature (London) **399**, 560 (1999).

[27] A. Moreo, M. Mayr, A. Feiguin, S. Yunoki, and E. Dagotto, Phys. Rev. Lett. **84**, 5568 (2000).

[28] M. Mayr, A. Moreo, J. A. Verges, J. Arispe, A. Feiguin, and E. Dagotto, Phys. Rev. Lett. **86**, 135 (2001).

[29] T. Nakajima, H. Kageyama, H. Yoshizawa, and Y. Ueda, J. Phys. Soc. Jpn. **71**, 2843 (2002).

[30] Y. Ueda and T. Nakajima, J. Phys. Condens. Matter **16**, S573 (2004).

[31] Y. Motome, N. Furukawa, and N. Nagaosa, Phys. Rev. Lett. **91**, 167204 (2003).

[32] R. Kajimoto, H. Yoshizawa, H. Kawano, H. Kuwahara, Y. Tokura, K. Ohoyama, and M. Ohashi, Phys. Rev. B **60**, 9506 (1999).

[33] A. I. Kurbakov, A. V. Lazuta, and V. A. Ryzhov, J. Phys. Conf. Ser. **200**, 012099 (2010).

[34] Y. Tomioka, R. Kumai, T. Ito, and Y. Tokura, Phys. Rev. B **80**, 174414 (2009).

[35] Y. Tomioka and Y. Tokura, Phys. Rev. B **66**, 104416 (2002).

[36] Y. Tomioka, H. Hiraka, Y. Endoh, and Y. Tokura, Phys. Rev. B **74**, 104420 (2006).

[37] M. Dlouha, S. Vratislav, Z. Jirak, J. Hejtmanek, K. Knizek, and D. Sedmidubsky, Appl. Phys. A **74**, S673 (2002).

[38] S. Chatterjee and A. K. Nigam, Phys. Rev. B **66**, 104403 (2002).

[39] P. Schiffer, A.P. Ramirez, W. Bao, and S.-W. Cheong, Phys. Rev. Lett. **75**, 3336 (1995); P. G. Radaelli, D. E. Cox, M. Marezio, and S-W. Cheong, Phys. Rev. B **55**, 3015 (1997).

[40] H. Fujishiro, M. Ikebe, and Y. Konno, J. Phys. Soc. Jpn. **67**, 1799 (1998).

[41] H. Kuwahara, Y. Moritomo, Y. Tomioka, A. Asamitsu, M. Kasai, R. Kumai, and Y. Tokura, Phys. Rev. B **56**, 9386 (1997).

[42] H. Kuwahara, Y. Tomioka, A. Asamitsu, Y. Moritomo, and Y. Tokura, Science **270**, 961 (1995).

[43] H. Kuwahara, T. Okuda, Y. Tomioka, A. Asamitsu, and Y. Tokura, Phys. Rev. Lett. **82**, 4316 (1999).

[44] H. Kawano, R. Kajimoto, H. Yoshizawa, Y. Tomioka, H. Kuwahara, and Y. Tokura, Phys. Rev. Lett. **78**, 4253 (1997).